19

High Reliability Alumina-Silicon Carbide Laminated Composites by Spark Plasma Sintering

Vincenzo M. Sglavo and Francesca De Genua
University of Trento
Italy

1. Introduction

High-melting temperature oxides, carbides and nitrides (Al_2O_3, ZrO_2, SiC, B_4C, Si_3N_4, BN) are superior in hardness and strength to metals, especially at high temperature and in severe conditions. However, the extensive use of such ceramics in structural engineering applications often encountered critical problems due to their lack of damage tolerance ability and to the limited reliability of the mechanical properties.

Several ceramic composites and, in particular, laminated structures were developed in recent years to enhance strength, toughness and to improve flaw tolerance. Fracture resistance and R-curve behaviour were achieved in laminated composites with (i) thin layers in residual compression alternated to thick layers in tension able to arrest surface and internal cracks and produce a threshold strength (Rao et al., 1999; Orlovskaya et al., 2005; Bermejo et al., 2006; Bermejo & Danzer, 2010; Náhlík et al., 2010), (ii) weak or porous interlayers that generate graceful and tortuous crack propagation paths (Davis et al., 2000; She et al., 2000), (iii) high strength surface layers and high toughness core, able to arrest starting surface flaws and to limit long cracks propagation, respectively, (Cho et al., 2001) and (iv) metallic layers that promote ductile bridging effects (Mekky & Nicholson, 2007).

The limitations of such laminates are related to processing difficulties and to the fact that they can be used only when the tensile load is applied parallel to the layers, thus being not easily suitable to produce real components such as shells or tubes. Nevertheless the improvement in toughness is often achieved at the expense of strength and still leaves limited relief from the variability in fracture stress.

Both significant strength increase and improved mechanical reliability, in terms of Weibull modulus or minimum threshold failure stress, can be achieved by the "engineering" of the critical surface region in the ceramic component. Such effect can be realized by using a laminated composite structure with tailored sub-surface insertion of layers with different composition. Such laminate is able to develop, upon co-sintering, a spatial variation of residual stress with maximum compression at specific depth from the surface due to the differences in thermal expansion coefficient of the constituting layers. The arising apparent fracture toughness curve (Sglavo et al., 2001; Sglavo & Bertoldi, 2006 a; Sglavo & Bertoldi, 2006 b) is responsible for the stable growth of surface flaws before final catastrophic failure

and, consequently, for a certain surface damage insensitivity that leads to outstanding mechanical reliability. Using this approach, some oxide laminated structures have been produced by tape casting, a convenient and well-developed technique for the preparation of thin green sheets, and pressureless sintering and in most cases very high reliability has been observed experimentally. (Sglavo et al., 2005; Costabile & Sglavo, 2006; Sglavo & Bertoldi, 2006 a; Sglavo & Bertoldi, 2006 b; Leoni et al, 2008).

In the present work silicon carbide has been selected as second phase to graduate the thermal expansion coefficient of alumina due to its relatively low specific density that could allow the production of lighter components with improved mechanical performance and reliability. Silicon carbide, in the shape of particle, nanoparticle, platelet or whisker, has been used many times in the past to improve hardness, strength, toughness, thermal shock resistance and creep resistance of alumina ceramics (Lee & Rainforth, 1994; Peters, 1998) Nevertheless, it has been shown that pressureless sintering to full density of alumina/silicon carbide composites can occur only at temperatures above 1700°C and usually involves considerable weight loss due to the formation of volatile compounds (Gadalla et al., 1992; Hue et al., 1997). In order to overcome such problems the alumina/silicon carbide composites have been usually prepared by pressure assisted sintering techniques such as Hot Pressing (HP).

In the present work, Spark Plasma Sintering (SPS) technology has been chosen for the consolidation of the laminates. SPS is a new promising solid compressive and pulsed electric current energizing sintering technology whose consolidation mechanisms are still under debate. During the SPS process a mechanical pressure is applied to the powder compact within the die while heating is provided internally thanks to a pulsed direct electric current passing through the die and, depending on the electrical conductivity of the material to be sintered, also through the powder compact. Such electrical current propagation significantly improves heat-transfer resulting in a current activated sintering. Therefore, SPS has several advantages over conventional sintering methods including higher heating rates, lower processing temperatures and shorter holding times, this allowing the production of highly dense materials with good control of grain coarsening (Chae et al., 2006; Munir et al., 2006).

The purpose of this work was to produce by tape casting and SPS alumina/silicon carbide monolithic composite laminates, made by stacking together laminae of identical composition, and an engineered laminate, with layers of different composition, specifically designed to manifest high mechanical reliability.

2. Experimental

2.1 Sample Processing

Commercially available high-purity α-Al_2O_3 (A-16SG, Alcoa Inc., Pittsburgh, PA, USA) and α-SiC (Sika ABR I F1500S, Saint-Gobain, Courbevoie, France) powders with average particle size of 0.4 μm and 1.8 μm and specific surface area of 8.6 m^2/g and 4.9 m^2/g, respectively, were used in this work.

Alumina/silicon carbide laminae with 0 ÷ 30 vol% SiC loads were produced and labelled as ASx where x is the volume content of the second phase (SiC). The green laminae were obtained by tape casting of water–based slurries prepared using a two-stage milling/mixing procedure necessary to break up powder agglomerates and to maintain the mechanical and chemical stability of the used binders. The alumina slurry was firstly prepared by mixing

the powder to deionized water with ammonium polymethacrylate as dispersant (Darvan C®, R. T. Vanderbilt Inc., Norwalk, CT, USA) - 0.4 mg/m^2 of active matter per unit area of alumina powder - for 24 h with alumina milling media. Then SiC powder was added and the dispersion was mixed for additional 24 h. The SiC powder was electrostatically dispersed so that no further amount of a dispersant was required.
The slurry was filtered through a 41 μm filter and de-aired for 30 min using a low-vacuum Venturi pump to remove air entrapped during the milling stage. An acrylic emulsion (Duramax® B-1014, Rohm & Hass, Philadelphia, PA, USA) as binder and a low-Tg acrylic emulsion (Duramax ® B-1000, Rohm & Hass, Philadelphia, PA, USA) as plasticizer were added to the dispersions and mixed for 30 min, taking care to avoid the production of new air bubbles. Three drops of 10 wt% wetting agent water solution (NH_4-lauryl sulphate, code 09887, Fluka Chemie AG, Buchs, Switzerland) were also added after 20 min of mixing to improve the tape spread onto the casting substrate. All suspensions were produced with a powder content equal to 39 vol%. Binder content was always equal to 15.3 vol% and plasticizer was added in a volume ratio equal to 1:2 with respect to the binder.
Tape casting was carried out using a double doctor-blade assembly (DDB-1-6, 6 in wide, Richard E. Mistler Inc., Yardley, PA, USA) with a gap height of 250 μm at a speed of 1 m/min. The tapes were casted on the polyethylene hydrophobic surface side of a composite film substrate (PET12/Al7/LDPE60, BP Europack, Vicenza, Italy) fixed on a rigid float glass plate. The relative humidity of the over-standing environment was set to 80%, after casting, in order to control the tapes drying. Green tapes with smooth surfaces and a uniform thickness of about 120 μm were therefore produced. Disks of 20 mm diameter were cut from the tapes by a hollow punch.
Green laminates were produced by thermo-compressing in a 20 mm nominal diameter aluminium die with a predefined stacking of 60 disks at 80°C under 30 MPa for 15 min.
According to the results of the thermogravimetric analysis (STA409 Netzsch GmbH, Bayern, Germany), performed at 5°C/min in air on binders and SiC powder, the adopted debinding heating cycle to allow slow and complete burn-out of organic additives was 1°C/min up to 600°C; the temperature was then raised to 4°C/min up to 1000°C for the successive pre-sintering treatment (dwell time = 12 min) useful to produce samples that could be easily handled without noticeable oxidation of the carbide.
Each pre-sintered laminate measuring 20 mm in diameter and 5.8-6.1 mm in height was wrapped into a graphite foil and carefully placed into the graphite mold. This latter was then closed and placed in the SPS apparatus (Dr. Sinter 1050, Sumimoto Coal Mining Co., Tokyo, Japan). A preliminary uniaxial pressure equal to 6.4 MPa was applied at room temperature. Vacuum level of 10^{-2} mbar was reached and pulsed current (12 impulses of 3 ms on and 2 impulses of 3 ms off) was applied. The temperature was raised up to 600°C in 5 min and then monitored and regulated by means of an optical pyrometer. Then the uniaxial pressure was risen to 28.7 MPa and the temperature was increased at first up to 1650°C (heating rate = 100°C/min) and then to 1700°C (heating rate = 50°C/min). After a holding time of 5 min the pressure was released, the current was turned off and the sample was cooled down.
Graphite foil residues were eliminated from the 3.2-3.4 mm thick sintered laminates by grinding on 250 μm grit diamond disks. A graphite spray was also used to protect the surfaces of the engineered laminates (that realized with laminae of different composition, as

reported below) during SPS, and no grinding procedure was used to remove graphite residues from such surfaces.

2.2 Design of the Engineered Laminate

Layers with different composition were stacked to obtain, after SPS, the architecture of the engineered laminate shown in Fig. 1 and labelled as AS-1. Such architecture was selected on the basis of the results presented in previous works to guarantee the stable growth of surface cracks before final failure (Sglavo et al., 2005; Costabile & Sglavo, 2006; Sglavo & Bertoldi, 2006 a; Sglavo & Bertoldi, 2006 b).

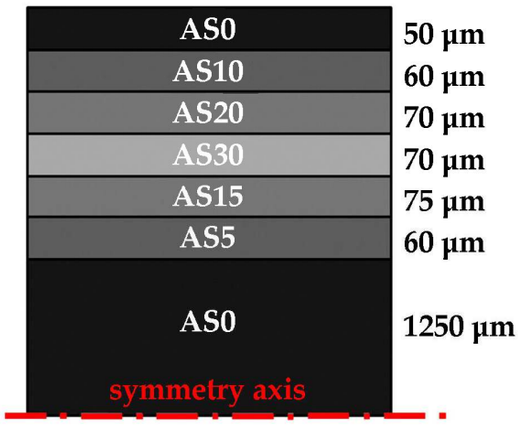

Fig. 1. Architecture (i.e. composition, stacking order and layers thickness) of the engineered alumina/silicon carbide multilayer. Dimensions are not in scale.

Sintering of a ceramic composite laminate made of layers of different composition is responsible for the formation of biaxial residual stresses in the laminate. During cooling, the difference in elastic modulus and, most of all, thermal expansion coefficient of the constituent layers is accommodated by diffusion mechanisms as long as the temperature is high enough (Rao et al., 2001). Below a certain temperature, T_{SF}, which is called the "stress free" temperature, the different components behave like a perfect elastic solid and internal stresses appear. The residual stresses $\sigma_{res,i}$ within each single layer (rank = i) under the hypotheses of symmetrical laminate geometry and perfect adhesion between layers, can be calculated using the following equation (Sglavo et al., 2005; Sglavo & Bertoldi, 2006 a; Sglavo & Bertoldi, 2006 b):

$$\sigma_{res,i} = E_i^*(\overline{\alpha} - \alpha_i)(T_{SF} - T_{RT}) \quad (1)$$

where T_{RT} is the room temperature and:

$$E_i^* = \frac{E_i}{1 - \upsilon_i} \quad (2)$$

E_i being the elastic modulus and υ_i the Poisson's ratio.
The average thermal expansion coefficient $\overline{\alpha}$ of the whole laminate, is:

$$\overline{\alpha} = \frac{\sum_{i=1}^{n} E_i^* t_i \alpha_i}{\sum_{i=1}^{n} E_i^* t_i} \tag{3}$$

t_i being the layer thickness and n the total number (odd) of the layers.
The effect of residual stresses on fracture behaviour can be combined with the intrinsic fracture toughness of each layer K_c^i thus obtaining the so-called apparent fracture toughness as a function of the distance from the surface, i.e. for increasing crack depths, (Sglavo et al., 2005; Sglavo & Bertoldi, 2006 a; Sglavo & Bertoldi, 2006 b):

$$T = K_C^i - \sum_{j=1}^{i} \left[2Y \left(\frac{c}{\pi} \right)^{0.5} \Delta\sigma_{res,j} \left[\frac{\pi}{2} - \arcsen\left(\frac{x_{j-1}}{c} \right) \right] \right] \qquad x_{i-1} < x < x_i \tag{4}$$

where $Y \approx 1.1215$, $\Delta\sigma_{res,j}$ being the stress increase of layer i with respect to the previous one, x_j the starting depth of layer j.
Equation (4) represents a short notation of n different equations, the sum being calculated for different number of terms for each i. On the basis of such approach, once the crack model is defined, the material failure is determined by comparing T with the stress intensity factor associated to the external loads only.
The properties of alumina and silicon carbide required for the design calculations can be obtained from NIST Structural Ceramics Database (www.nist.gov). Young modulus (E) and Poisson's ratio (υ) values for monolithic alumina/silicon carbide composites are calculated as the Hashin-Shtrikman bounds (Kingery et al., 1976) and thermal expansion coefficient (α) is evaluated by the Kerner equation (Kingery et al., 1976). Hardness (H) and fracture toughness (K_C) were determined by the conventional indentation fracture method (Anstis et al., 1972). Vickers indentations were produced using a load of 100 N for 15 s.
The properties of the composite materials used in the design procedure are summarized in Table 1. The reported thickness corresponds to the average actual value measured on optical micrographs of polished fracture surface of the sintered engineered laminate.

	AS0	AS5	AS10	AS15	AS20	AS30
K_C [MPa $m^{0,5}$]	3.73	2.61	2.80	2.87	3.04	2.99
E [GPa]	415.9	415.9	416.0	416.1	416.1	416.2
υ	0.23	0.227	0.224	0.22	0.217	0.21
α (0÷1000°C) [10^{-6} °C^{-1}]	8.1	7.98	7.85	7.72	7.59	7.32
thickness [μm]	52	57	57	75	67	66

Table 1. Materials properties and layers thickness used to estimate the stress distribution and the apparent fracture toughness of the engineered laminate AS-1. The thickness corresponds to the average actual value measured on the sintered samples.

The resulting residual stress profile calculated according to Eq. (1) for the engineered laminate AS-1 is shown in Fig 2. A stress free temperature equal to 1200°C was used for the calculations. Similarly to previous situations where the material was tailored to manifest high mechanical reliability (Green et al., 1999; Sglavo & Green, 2001; Sglavo et al., 2005; Costabile & Sglavo, 2006; Sglavo & Bertoldi, 2006 a; Sglavo & Bertoldi, 2006 b; Leoni et al, 2008), the stress state is slightly tensile (around 50 MPa) on the surface while a considerable residual compression (in excess to 400 MPa) occurs at a certain depth in the fourth layer.

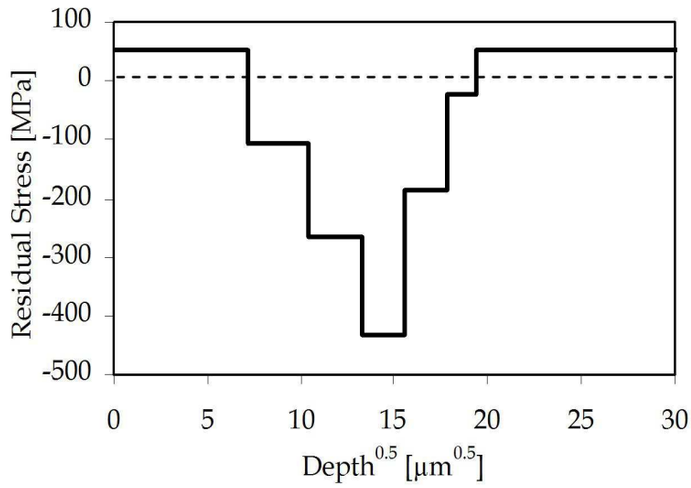

Fig. 2. Calculated residual stress profile in the surface region of the engineered laminate AS-1.

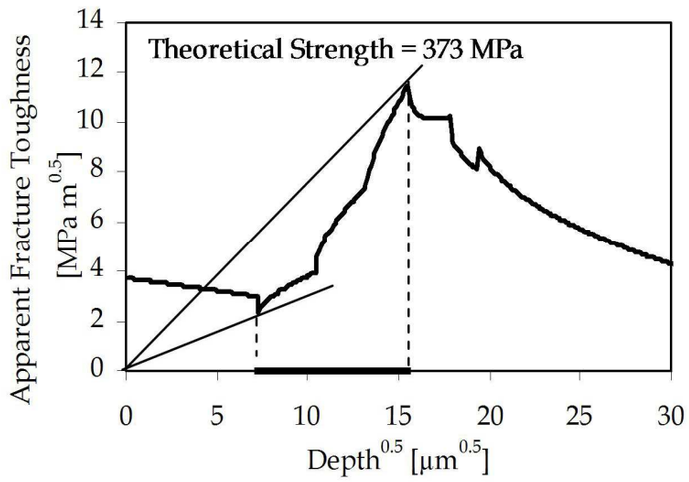

Fig. 3. Apparent fracture toughness for the engineered laminate AS-1. The straight line corresponding to the design failure stress and the minimum stress required for crack propagation are also shown and used for the determination of the stable growth interval (horizontal bar).

The apparent fracture toughness, T, of the laminate due to this stress profile and calculated according to Eq. (4) is shown in Fig. 3 as a function of the distance from the surface. A wide stable crack growth interval (from ≈ 12 μm to ≈ 250 μm) before final failure, that could be responsible for limited strength variability, can be observed. The failure stress associated to the maximum apparent fracture toughness, graphically determined by the line intersecting T at the maximum, is equal to ≈ 375 MPa.

2.3 Sample characterization

Green compact porosity and pore size distribution were measured by mercury porosimetry on the pre-sintered laminates (Pascal 140 and Porosimeter 2000, CE Instruments, Milano, Italy). The relative densities of the sintered samples were measured by the Archimedes technique using distilled water as immersion medium. The theoretical densities of the composites were calculated by the rule of mixtures assuming a value of 3.984 g/cm^3 for Al_2O_3 and 3.16 g/cm^3 for SiC.

X-ray diffraction (XRD) analyses (Geiger Flex Dmax III, Rigaku Inc., Tokyo, Japan) were carried out on monolithic pre-sintered and sintered laminates.

Fracture strength of all the laminates was measured by piston-on-three-balls biaxial flexural test (Shetty et al., 1980) using a universal mechanical testing machine (mod. 810, MTS Systems, Minneapolis, MN, USA). The disks were supported by three steel balls (3.2 mm diameter) lying on a circle (12.4 mm diameter) 120° apart. The load was applied at the centre by a hardened steel cylinder (1.5 mm diameter). A certain number of AS-1 engineered laminates were also pre-cracked in the center of the prospective tensile face by Vickers indentation using loads ranging from 10 N to 100 N before flexural test.

Fracture surfaces were finally examined by optical (BH2-UMA, Olympus Optical Co. GmbH, Hamburg, Germany) and scanning electron microscopy (JSM-5500, Jeol Inc., Tokyo, Japan). The average grain size was measured by the linear intercept method (Wurst & Nelson, 1972) on optical and scanning electron micrographs. A minimum of 200 grains from 5 randomly selected areas were counted for each sample. To reveal the microstructure specimens were diamond polished to 1 μm to obtain a mirror finish and etched: alumina was thermally etched at 1500°C for 20 min in air, while the composites were chemically etched in phosphoric acid at 250°C for 3 min.

3. Results and Discussion

The pre-sintered monolithic laminates exhibited a total porosity of approximately 40% (Fig. 4) with narrow pore size distributions from 0.14 μm to 0.16 μm. The packing density and quality of green samples is high enough to help the sintering of the compacts. Successive SPS treatment allowed to produce dense composite materials (97-99% relative density). The addition of non sinterable inclusions of SiC to alumina determined a reduction of the bulk density without noticeable influence on the sintering of the composites that always reach almost theoretical density as shown in Fig. 4.

XRD analysis performed on AS0 and AS30 monolithic laminates did not point out the presence of any impurity and confirmed the expected composition by showing only α-Al_2O_3 peaks for the first one and α-Al_2O_3 and α-SiC peaks for the second one. The formation of mullite is very limited considering the amount of silica normally present as surface layer on SiC powder or formed during the pre-sintering step. The relevant change in colour of the

final samples from white, in the case of pure alumina, or light grey to black revealed that a non-controlled small carbon amount is introduced during the SPS process probably from the graphitic foil and apparatus. It is not a surface contamination but it is included deep inside within the samples.

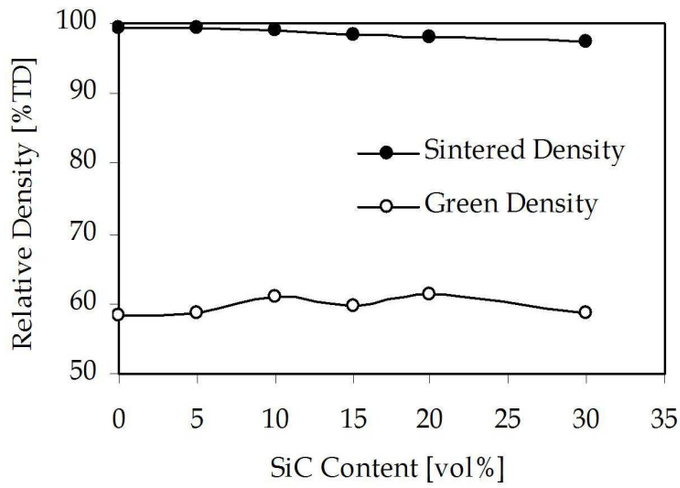

Fig. 4. Pre-sintered and sintered relative density as a function of SiC content in the monolithic laminates. The theoretical densities (TD) of the composites were calculated by the rule of mixtures assuming a value of 3.98 g/cm^3 for Al_2O_3 and 3.16 g/cm^3 for SiC.

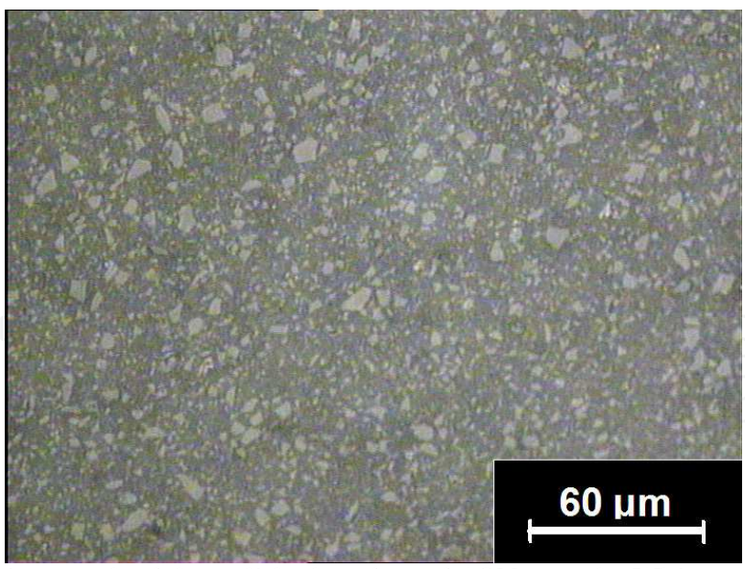

Fig. 5. Optical micrograph of the polished surface of AS30 sample. White particles represent silicon carbide.

Microscopical observations of the laminates polished surface confirmed the presence of limited porosity and revealed a homogeneous distribution of the two phases as shown in Fig. 5. Perfect adhesion between the initial layers was also observed both in monolithic and

engineered laminates (Fig. 6) where layers of different composition were assembled; this confirms the goodness and the reliability of the processing procedure used in the present work.

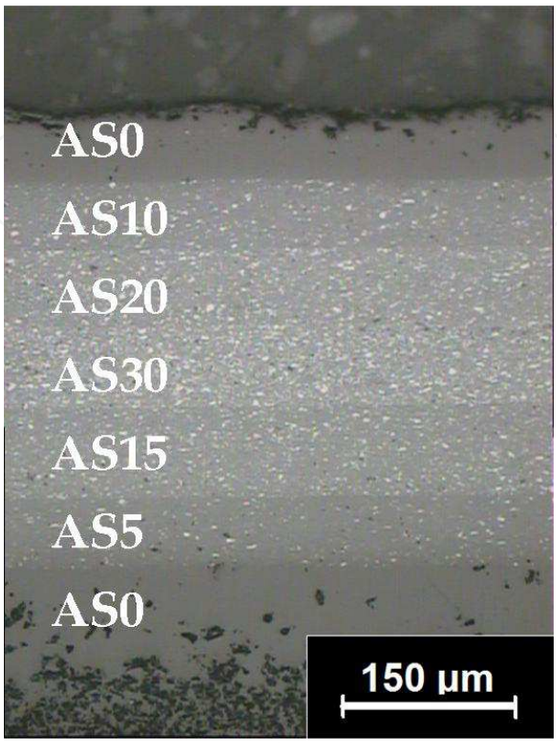

Fig. 6. Optical micrograph of the polished surface of AS-1 sample. Perfect adhesion between the layers of different composition can be observed.

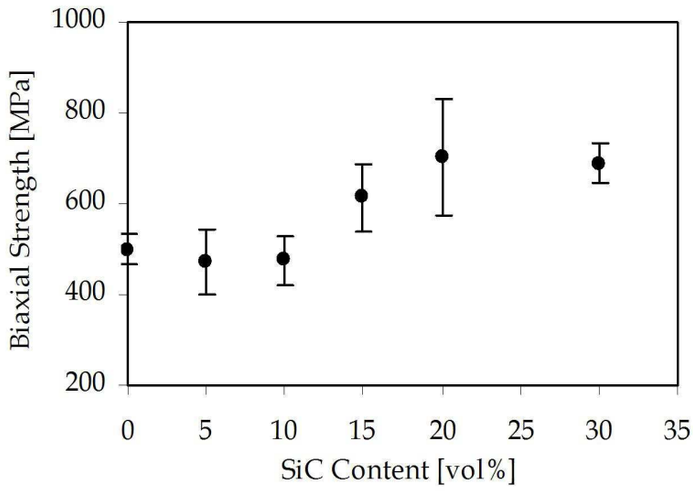

Fig. 7. Strength of monolithic laminates.

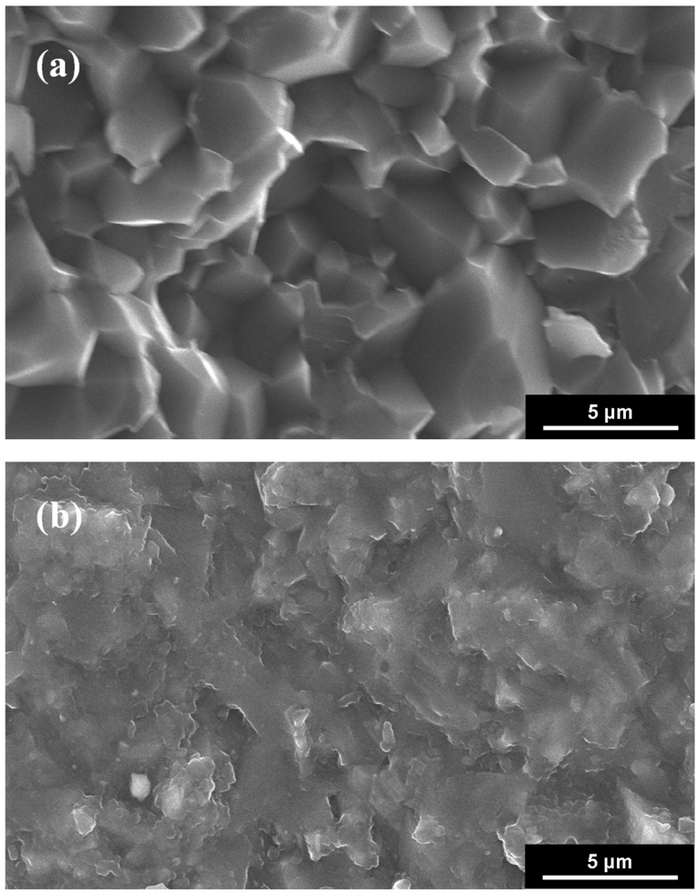

Fig. 8. Fracture surface of AS0 (a) and AS30 (b) monolithic laminates.

Grain size distribution is not homogeneous in monolithic alumina and 1 µm grains were observed as well as some larger 10 µm grains. However, the alumina mean grain size ranges from 6.9±0.5 µm in the pure alumina monolithic laminate to approximately 1 µm in the monolithic 30 vol% SiC containing composite. On the other hand, silicon carbide grain size is equal to 4.2±0.3 µm in all monolithic composites. The alumina grain refinement in the composites has been already reported in literature and has been attributed to a decreased grain boundary mobility, diffusivity and rate of densification due to SiC particles presence (Chae et al., 2006).

The strength measured on monolithic laminates is shown in Fig. 7. The addition of limited amount of SiC, up to 10 vol%, does not affect the strength of the composite which exhibits the resistance of pure alumina, around 500 MPa. For silicon carbide loads exceeding 10 vol% an appreciable increase of the biaxial failure stress is observed and values as high as 700 MPa are obtained for SiC content of 20 and 30 vol%. The standard deviation shown for all monolithic samples is always quite large due to the limited number of samples, four to five, used for the mechanical tests. Only for pure alumina ten samples were used. The observed increase in failure stress with SiC content can be accounted for by the transformation of the fracture propagation from intergranular in pure alumina samples to transgranular in composites containing larger amount of silicon carbide as shown in Fig. 8; such effect of

matrix weakening and grain boundary strengthening is in good agreement with findings reported in previous works (Levin et al., 1995; Sternitzke, 1997; Pérez-Riguero et al., 1998) and is a consequence of the tensile residual stresses field which develops upon cooling in the matrix around SiC particles because of the thermo-elastic mismatch between Al_2O_3 and SiC. The reduction of critical defect size associated to smaller grain size obtained with SiC additions, that inhibit the grain growth of Al_2O_3, can also be considered for the observed increase of strength.

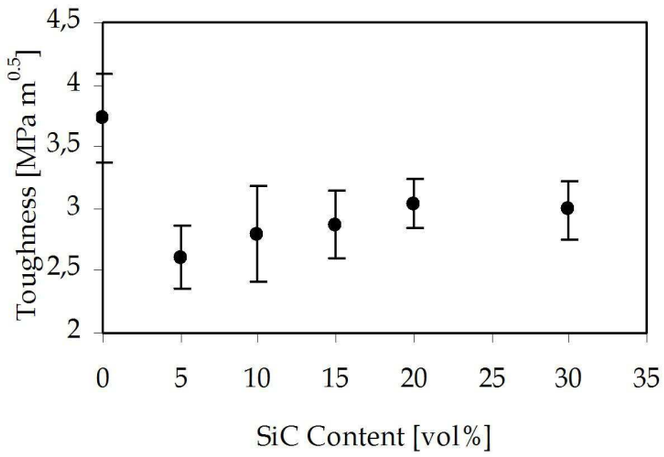

Fig. 9. Toughness of monolithic laminates.

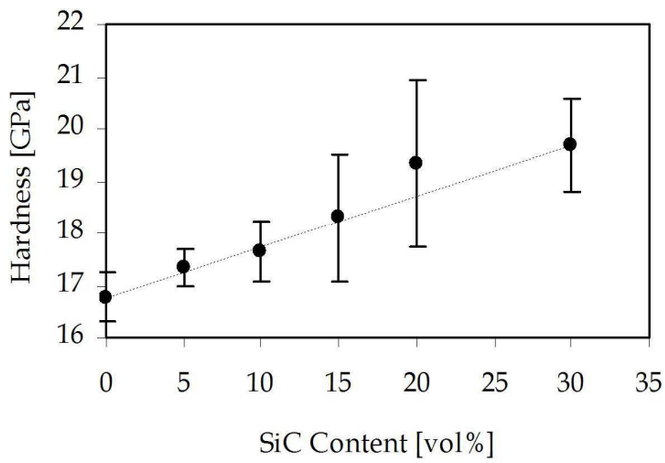

Fig. 10. Hardness of monolithic laminates. The straight line represents the values calculated by the rule of mixture.

As shown in Fig. 9 all monolithic composites show toughness values lower than those of alumina independently on the added SiC volumetric fraction and despite the change in fracture mode. The fracture mode change from intergranular in pure alumina to

transgranular in the composites (Fig. 8) seems to be not effective in the present case. Conflicting results and theories are reported in literature about the grain boundary strengthening and toughening, especially in the case of Al_2O_3/SiC nanocomposites (Pérez-Riguero et al., 1998). Through a simple comparison of the experimental values, one can concludes that the average tensile stress field in the alumina matrix due to the thermal expansion mismatch of alumina and SiC reduces the fracture toughness more than the increase due to the change in the fracture mode. A net increase in toughness can be achieved only in the case the average internal stresses are small (Carrol et al., 1996).
All composites show an increase of hardness over monolithic alumina (Fig. 10). The experimental trend is comparable to a linear rule of mixture assuming values of 16.8 GPa and 26.5 GPa for pure alumina and silicon carbide respectively.

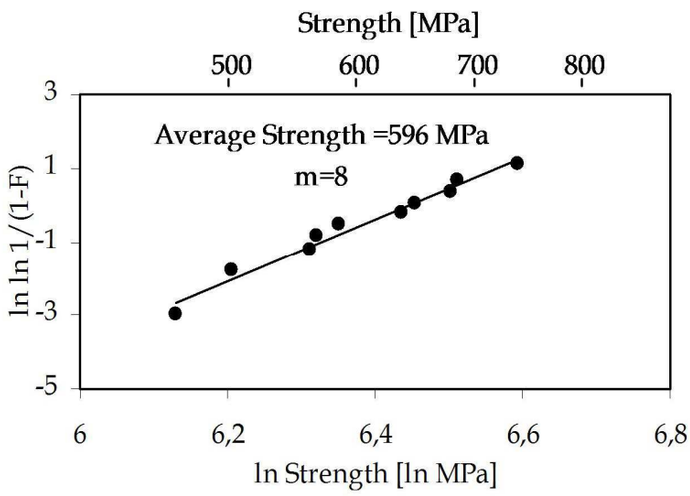

Fig. 11. Weibull diagram for the engineered laminate AS-1. The straight line represents best linear fitting of the experimental data.

The biaxial bending strength measured on the engineered laminate AS-1 is graphically represented on the Weibull plot in Fig. 11. The fracture probability, F, was calculated as F = (j-0.5)/N where N is the total number of samples and j the rank in the ascending ordered distribution. The linear fitting of the experimental data allows the determination of the Weibull modulus, m, equal to 8.3. The average strength is equal to 596 ± 85 MPa.
It is now useful to compare the obtained results with the design strength that can be evaluated on the basis of the chosen laminate architecture. There is a substantial difference between the experimental average strength (596 MPa) and the design failure stress (373 MPa); even the weakest sample in the Weibull distribution shown in Fig. 11 possesses a strength of 460 MPa, definitely higher than the design stregth. These observations require some explanation. The outer layer of AS-1 laminate is made of pure alumina. Therefore, the dimension of surface cracks can be estimated from the fracture toughness and the strength measured on alumina specimens that range from 26 to 38 μm if semi-circular cracks are supposed. This means that, in spite of the simplifications made in the model and in the calculations, on the basis of Fig. 3, surface flaws in AS-1 laminate should undergo to stable growth upon bending before final catastrophic failure. Nevertheless, since the T curve is

very steep before its maximum, after an initial growth in the depth, surface flaw could propagate more easily along the surface, evolving at first from semi-circular to semi-elliptical and then to through-thickness crack. Careful observation of fracture surfaces allows to confirm such hypothesis.

Examination of fractographic features of monolithic alumina samples shows typical crack patterns of biaxial moderate strength with bent mirror and main crack branching soon after the mirror boundaries. The samples break into 3÷5 fragments, with a quite clear-cut and planar fracture surface (Fig. 12). The engineered laminate shows a more extensive fragmentation due to more intensive stress state. All samples possess fracture surfaces with more complex crack propagation, involving steps and jogs in the mirror and excursion of the crack front out of the plane in proximity of the surface in tension (Fig. 13). Crack propagation occurs initially orthogonally to the surface in tension but then kinks as it approaches the highly compressed layers.

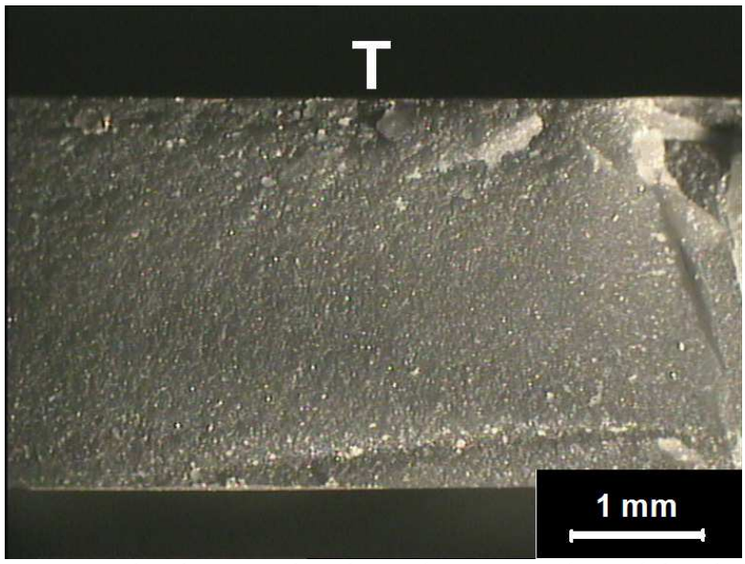

Fig. 12. Optical micrographs showing the planar fracture surface of the alumina monolithic laminate. The surface in tension in the flexure test is marked with T.

This effect is evident in Fig. 14 that corresponds to a polished section of a sample subjected to biaxial bending where a surface crack initially propagates perpendicularly to the surface in tension and then deviates tilting out from the main fracture plane once encountering high intensity biaxial residual compressive stresses.

In addition, SEM micrograph (Fig. 15) taken on the fracture surface in proximity of the surface in tension shows a smooth region extending along ≈ 400 μm from the surface due to a stable crack growth of defects in the residual compressive field. Similar peculiar crack propagation behaviour has already been observed in pre-stresses ion-exchanged glasses (Sglavo et al., 2007) where, similarly to the engineering process used in the present work, a specific residual stress field with maximum compression at a certain depth from the surface was created (Green et al., 1999; Sglavo & Green, 2001).

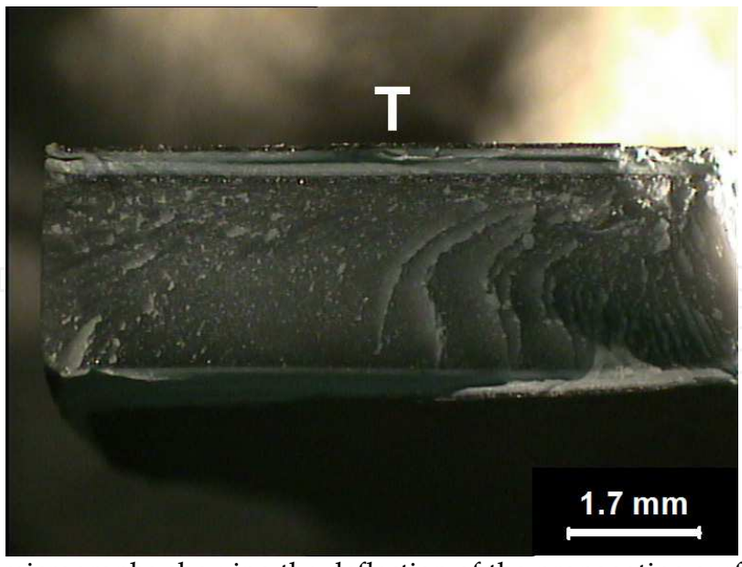

Fig. 13. Optical micrographs showing the deflection of the propagating surface crack on the as broken fracture surface of a fragment of the AS-1 laminate. The surface in tension in the flexure test is marked with T.

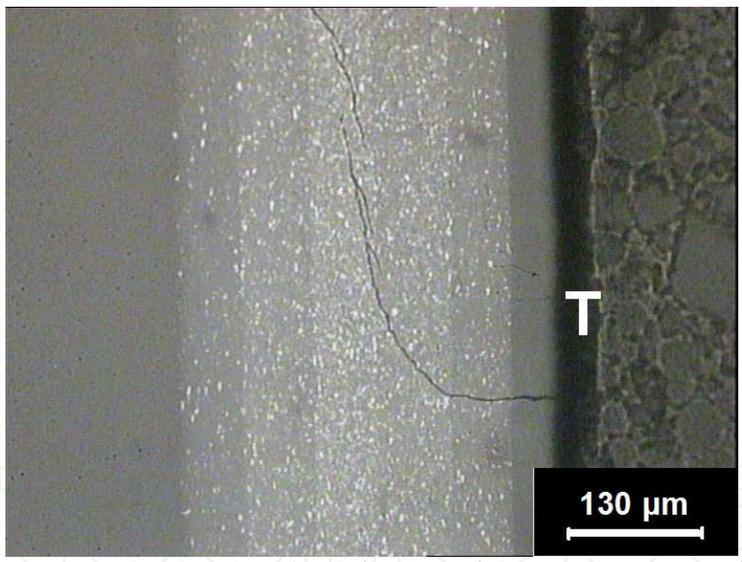

Fig. 14. Optical micrographs showing the deflection of the propagating surface crack on the polished fracture surface of a fragment of the AS-1 laminate. The surface in tension in the flexure test is marked with T.

This phenomenon is responsible for a shielding of the crack tip and consequently for higher failure stress. In addition, due to the randomness of such crack kink, the final strength is no more strictly controlled by the T-curve (Fig. 3) and becomes quite scattered. It is anyway interesting to observe that failure stress remains invariant even when large defects are introduced on the surface by Vickers indentation (Fig. 16). Strength values around 600 MPa are obtained even when indentation loads as high as 100 N, which produces radial cracks of the order of 100 µm, are used.

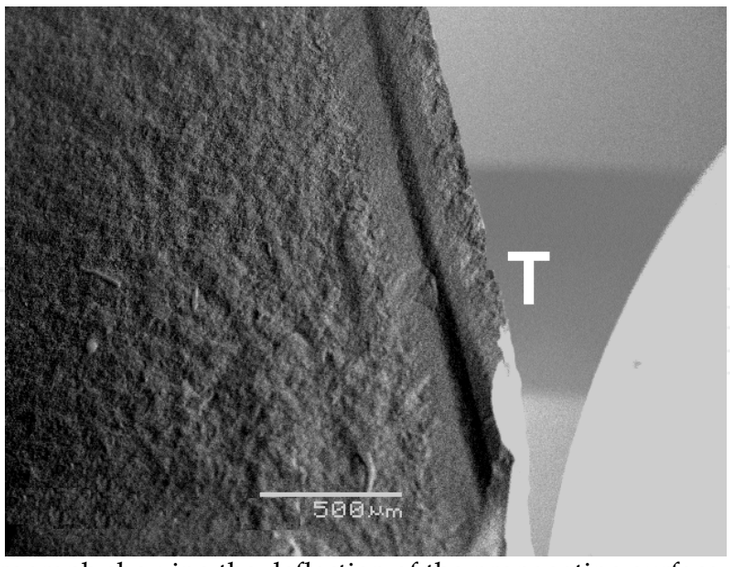

Fig. 15. SEM micrograph showing the deflection of the propagating surface crack at a certain depth. The surface in tension in the flexure test is marked with T.

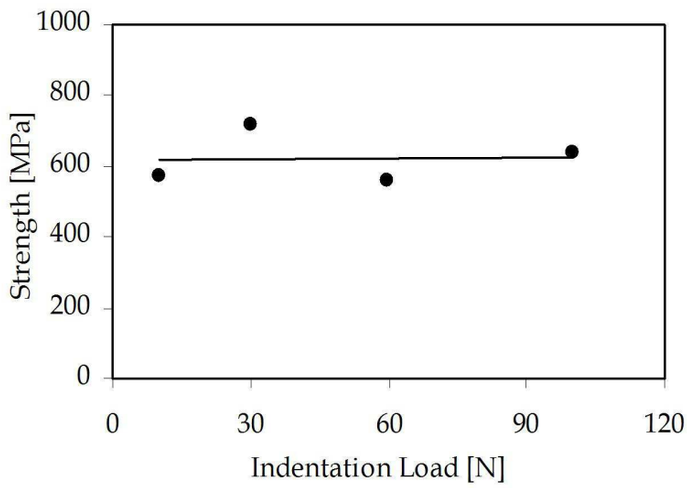

Fig. 16. Failure stress as a function of the indentation load for the engineered laminate.

4. Conclusion

Fully dense SiC-Al_2O_3 composites characterized by perfect adhesions between constituting layers were produced by Spark Plasma Sintering tape casted composite laminae.
Monolithic composite disks with SiC load up to 30 vol% and an engineered laminate with specific layers combination able to promote stable growth of surface defects before final failure were considered. High homogeneity of the two phases is always obtained.

Monolithic composites show an increasing strength with SiC content and biaxial failure stress as high as 700 MPa is obtained for the highest SiC load. A graceful crack propagation, first inward and then parallel to the surface of the laminate, can be observed in the engineered laminate. Such fracture behaviour is shown to be responsible for the high strength (about 600 MPa) and the peculiar surface damage insensitivity.

5. References

Anstis, G. R.; Chantikul, P.; Lawn, B. R & Marshall, D. B. (1981). A critical evaluation of indentation techniques for measuring fracture toughness: I, Direct crack measurements. *J. Am. Ceram. Soc.,* Vol. 64, No. 9, (September 1981) 533-538, ISSN 0002-7820

Bermejo, R.; Torres, Y.; Sanchez-Herencia, A. J.; Baudin, C.; Anglada, M. & Llanes, L. (2006). Residual stresses, strength and toughness of laminates with different layer thickness ratios. *Acta Mater.,* Vol. 54, No. 18, (October 2006) 4745–4757, ISSN 1359-6454

Bermejo, R. & Danzer, R. (2010). High failure resistance layered ceramics using crack bifurcation and interface delamination as reinforcement mechanisms. *Eng. Fract. Mech.,* Vol. 77, No. 11, (July 2010) 2126–2135, ISSN 0013-7944

Carroll, L.; Sternitzke, M. & Derby, B. (1996). Silicon carbide particle size effects in alumina-based nanocomposites. *Acta Mater.,* Vol. 44, No. 11, (November 1996) 4543-4552, ISSN 1359-6454

Chae, J. H.; Kim, K. H.; Choa, Y. H.; Matsushita, J.; Yoon, J.-W. & Shim, K. B. (2006). Microstructural evolution of Al_2O_3-SiC nanocomposites during spark plasma sintering. *J. Alloys Compounds,* Vol. 413, No. 1-2, (March 2006) 259-264, ISSN 0925-8388

Cho, K. S.; Choi, H. J.; Lee, J. G. & Kim, Y. W. (2001). R-curve behaviour of layered silicon carbide ceramics with surface fine microstructure. *J. Mater. Sci.,* Vol. 36, No. 9, (May 2001) 2189-2193, ISSN 0022-2461

Costabile, A. & Sglavo, V. M. (2006). Influence of the architecture on the mechanical performances of alumina-zirconia-mullite ceramic laminates. *Adv. in Science and Technology,* Vol. 45, (October 2006) 1103-1108, ISSN 1662-8969

Davis, J. B.; Kristoffersson, A.; Carlström E. & Clegg, W. J. (2000). Fabrication and Crack Deflection in Ceramic Laminates with Porous Interlayers. *J. Am. Ceram. Soc.,* Vol. 83, No. 10, (October 2000) 2369-2374, ISSN 0002-7820

Gadalla, A.; Elmasry, M. & Kongkachuichay, P. (1992). High temperature reactions within SiC-Al_2O_3 composites. *J. Mater. Res.,* Vol. 7, No. 9, (September 1992) 2585-2592, ISSN 0884-2914

Green, D. J.; Tandon R. & Sglavo, V. M. (1999). Crack arrest and multiple cracking in glass using designed residual stress profiles. *Science*, Vol. 283, No. 5406, (February 1999) 1295-1297, ISSN 0036-8075

Hue, F.; Jorand, Y.; Dubois, J. & Fantozzi, G. (1997). Analysis of the weight loss during sintering of silicon-carbide whisker-reinforced alumina composites. *J. Eu. Ceram. Soc.*, Vol. 17, No. 4, (February 1997) 557-563, ISSN 0955-2219

Kingery, W. D.; Bowen, H. K. & Uhlmann, D. R. (1976). *Introduction to ceramics*, J. Wiley & Sons, ISBN 0471478601, NY, pp. 603-606, pp. 773-777

Lee, W. E. & Rainforth, M. (1994). *Ceramic Microstructures – Property control by processing*, Chapman & Hall, ISBN 0412431408, London, U.K., pp. 509-570

Leoni, M.; Ortolani, M.; Bertoldi, M.; Sglavo, V. M. & Scardi, P. (2008). Nondestructive measurement of the residual stress profile in ceramic laminates. *J. Am. Ceram. Soc.*, Vol. 91, No. 4, (April 2008) 1218-1225, ISSN 0002-7820

Levin, I; Kaplan, W. D.; Brandon, D. G. & Layyous, A. A. (1995). Effect of SiC submicrometer particle size and content on fracture toughness of alumina-SiC "nanocomposites". *J. Am. Ceram. Soc.,* Vol. 78, No. 1, (January 1995) 254-256, ISSN 0002-7820

Mekky, W. & Nicholson, P. S. (2007). R-curve modeling for Ni/Al_2O_3 laminates. *Composites. Part B, Engineering*, Vol. 38, No. 1, (January 2007) 35-43, ISSN 1359-8368

Munir, Z. A.; Anselmi-Tamburini, U. & Ohyanagi, M. (2006). The effect of electric field and pressure on the synthesis and consolidation of materials: A review of the spark plasma sintering method. *J. Mater. Sci.,* Vol. 41, No. 3, (February 2006) 763-777, ISSN 0022-2461

Náhlík, L.; Šestáková, L; Hutar, P. & Bermejo, R. (2010). Prediction of crack propagation in layered ceramics with strong interfaces. *Eng. Fract. Mech.,* Vol. 77, No. 11, (July 2010) 2192–2199, ISSN 0013-7944

Orlovskaya, N.; Kuebler, J.; Subbotin, V. & Lugovy, M. (2005). Design of Si_3N_4-based ceramic laminates by the residual stresses. *J. Mat. Sci.,* Vol. 40, No. 20, (October 2005) 5443–5450, ISSN 0022-2461

Pérez-Riguero, J.; Pastor, J. Y.; Llorca, J.; Elices, M.; Miranzo, P. & Moya, J. S. (1998). Revisiting the mechanical behavior of alumina/silicon carbide nanocomposites. *Acta Mater.,* Vol. 46, No. 15, (September 1998) 5399-5411, ISSN 1359-6454

Peters, S. Y. edt. (1998). *Handbook of composites*, Chapman & Hall, ISBN 0412540207, London, U.K., pp. 307-332

Rao, M. P.; Sánchez-Herencia, A. J.; Beltz, G. E.; McMeeeking, R. M. & Lange, F. F. (1999). Laminar ceramics that exhibit a threshold strength. *Science,* Vol. 286, No. 5437, (October 1999) 102-105, ISSN 0036-8075

Rao, M. P.; Rödel, J. & Lange, F. F. (2001). Residual stress induced R-Curves in laminar ceramics that exhibit a threshold strength. *J. Am. Ceram. Soc.,* Vol. 84, No. 11, (November 2001) 2722-2724, ISSN 0002-7820

Sglavo, V. M.; Larentis, L. & Green, D. J. (2001). Flaw insensitive ion-exchanged glass: I, Theoretical aspects. *J. Am. Ceram. Soc.*, Vol. 84, No. 8, (August 2001) 1827-1831, ISSN 0002-7820

Sglavo, V. M. & Green, D. J. (2001). Flaw insensitive ion-exchanged glass: II, Production and mechanical performance. *J. Am. Ceram. Soc.,* Vol. 84, No. 8, (August 2001) 1832-1838. ISSN 0002-7820

Sglavo, V. M.; Paternoster, M. & Bertoldi, M. (2005). Tailored residual stresses in high reliability alumina-mullite ceramic laminates. *J. Am. Ceram. Soc.,* Vol. 88, No. 10, (October 2005) 2826–2832, ISSN 0002-7820

Sglavo, V. M. & Bertoldi, M. (2006 a). Design and production of ceramic laminates with high mechanical resistance and reliability. *Acta Mater.,* Vol. 54, No. 18, (October 2006) 4929-4937, ISSN 1359-6454

Sglavo, V. M. & Bertoldi, M. (2006 b). Design and production of ceramic laminates with high mechanical reliability. *Composites. Part B, Engineering,* Vol. 37, No. 6, (2006) 481-489, ISSN 1359-8368

Sglavo, V. M.; Prezzi, A. & Green, D. J. (2007). In situ observation of crack propagation in ESP (engineered stress profile) glass. *Eng. Fract. Mech.,* Vol. 74, No. 9, (June 2007) 1383-1398, ISSN 0013-7944

She, J.; Inoue T. & Ueno K. (2000). Damage resistance and R-curve behavior of multilayer Al_2O_3/SiC ceramics. *Ceram. Int.,* Vol. 26, No. 8, (2000) 801-805, ISSN 0272-8842

Shetty, D. K.; Rosenfield, A. R.; McGuire, P.; Bansal, G. K. & Duckworth, W. H. (1980). Biaxial flexure tests for ceramics. *Ceramic Bullettin*, Vol. 59, No. 12., (1980) 1193-1197, ISSN 002-7812

Sternitzke, M. (1997). Review: structural ceramic nanocomposites. *J. Eu. Ceram. Soc.,* Vol. 17, No. 9, (1997) 1061-1082, ISSN 0955-2219

Wurst, J. C. & Nelson, J. A. (1972). Linear intercept technique for measuring grain size in two-phase polycrystalline ceramics. *J. Am. Ceram. Soc.,* Vol. 55, No. 2, (February 1972) 109, ISSN 0002-7820

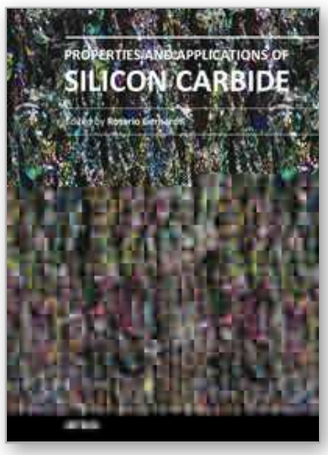

Properties and Applications of Silicon Carbide
Edited by Prof. Rosario Gerhardt

ISBN 978-953-307-201-2
Hard cover, 536 pages
Publisher InTech
Published online 04, April, 2011
Published in print edition April, 2011

In this book, we explore an eclectic mix of articles that highlight some new potential applications of SiC and different ways to achieve specific properties. Some articles describe well-established processing methods, while others highlight phase equilibria or machining methods. A resurgence of interest in the structural arena is evident, while new ways to utilize the interesting electromagnetic properties of SiC continue to increase.

How to reference
In order to correctly reference this scholarly work, feel free to copy and paste the following:

Vincenzo M. Sglavo and Francesca De Genua (2011). High Reliability Alumina-Silicon Carbide Laminated Composites by Spark Plasma Sintering, Properties and Applications of Silicon Carbide, Prof. Rosario Gerhardt (Ed.), ISBN: 978-953-307-201-2, InTech, Available from: http://www.intechopen.com/books/properties-and-applications-of-silicon-carbide/high-reliability-alumina-silicon-carbide-laminated-composites-by-spark-plasma-sintering

INTECH
open science | open minds

InTech Europe
University Campus STeP Ri
Slavka Krautzeka 83/A
51000 Rijeka, Croatia
Phone: +385 (51) 770 447
Fax: +385 (51) 686 166
www.intechopen.com

InTech China
Unit 405, Office Block, Hotel Equatorial Shanghai
No.65, Yan An Road (West), Shanghai, 200040, China
中国上海市延安西路65号上海国际贵都大饭店办公楼405单元
Phone: +86-21-62489820
Fax: +86-21-62489821

IntechOpen